Research Article

Aerogels from Fermented Peanut Shell Fiber with Improved Functional Properties and Oil Absorption Capacity

Huyen Ngoc Nguyen, Quyen Ho Minh Le and Ngoc Thanh Vu*
Department of Applied Chemistry, School of Biotechnology, International University, Ho Chi Minh City, Vietnam
Vietnam National University, Ho Chi Minh City, Vietnam

* Corresponding author. E-mail: vtngoc@hcmiu.edu.vn DOI: 10.14416/j.asep.2026.05.009
Received: 6 January 2026; Revised: 24 February 2026; Accepted: 29 April 2026; Published online: 28 May 2026
© 2026 King Mongkut's University of Technology North Bangkok. All Rights Reserved.

Abstract
Peanut shells, an abundant agricultural byproduct, present waste management challenges. This study investigated the impact of solid-state fermentation (SSF), an eco-friendly and cost-effective technique in waste valorization, on the chemical composition and structural properties of cellulose fiber derived from peanut shells and its subsequent utilization in aerogel production. Although the fiber yield remained unchanged after fermentation, compositional analysis revealed a substantial increase in the cellulose content of fermented peanut shell fiber (F-PSF) (from 59.1% to 71.8%). F-PSF also exhibited reductions in hemicellulose (from 17.3% to 9.3%) and lignin (from 13.7% to 8.6%) content. X-ray diffraction analysis indicated an increased crystallinity index of F-PSF, suggesting enhanced molecular ordering. Scanning electron microscopy showed a more fibrillated and less agglomerated structure of F-PSF, resulting in a better-defined porous network of F-PSF aerogel (F-PSFA). F-PSFA exhibited decreased density (from 0.033 g/cm³ to 0.019 g/cm³) and thermal conductivity (from 0.047 W/(m·K) to 0.039 W/(m·K)). Additionally, F-PSFA had increased porosity (from 90.3% to 96.1%), hydrophobicity (from 79.3° to 111.7° for water contact angle), and mechanical stability (from 4% to 36% size restoration after 9 compression times). Furthermore, F-PSFA demonstrated remarkable enhancements in oil absorption capacity (from 4–5 g/g to 21–25 g/g after 1-min absorption) and reusability (increasing from 1 g/g to 11 g/g after 9 cycles). These findings collectively highlight the effectiveness of SSF in processing peanut shells for producing aerogels with improved functional properties. These aerogels have pertinent applications in oil recovery, wastewater treatment, thermal insulation, and the biomedical field.

Keywords: Aerogel, Cellulose, Oil absorption, Peanut shell, Solid-state fermentation

1 Introduction

Aerogels have emerged as a highly promising and versatile material in many fields. They can be derived from various sources, such as metal oxides, synthetic polymers, silica, and cellulose. Compared to synthetic sources, cellulose offers particularly compelling solutions. As the most abundant natural polymer on Earth, cellulose is a sustainable, renewable, and biodegradable source for producing aerogels. It is a linear, unbranched polysaccharide composed of β-D-glucose units linked by β(1→4)-glycosidic bonds. Cellulose materials have exceptional properties, including high porosity, a large surface area, and remarkable adsorption capacities. They also have the potential to enhance energy efficiency in applications such as thermal insulation, wastewater treatment, drug delivery, and medical devices [1]–[5].

Cellulose can be extracted directly from fiber-rich sources or biosynthesized by microorganisms. One sustainable source for cellulose extraction is agricultural waste. Although agricultural waste biodegradation contributes essential plant nutrients and enhances soil porosity, a considerable amount of agricultural waste is incinerated for rapid disposal. This practice releases greenhouse gases and poses significant environmental and health risks [6], [7]. The peanut shell (PS) is a popular agricultural byproduct containing high levels of lignocellulosic components, including 32–48% cellulose, 3–21% hemicellulose,

and 26–36% lignin [8]. With global production exceeding 50 million tons annually, the resulting PS presents an environmental challenge, but it is also a substantial bioresource for cellulose aerogel production due to its high cellulose content [9].

Most studies on agricultural waste-derived cellulose aerogels involve recovering cellulose fiber using chemical and physical methods [4]. Prominent chemical treatments include the use of acidic, alkaline, and oxidative agents. Physical treatments commonly employ mechanical comminution, steam explosion, or hydrothermal treatment. In contrast, using biological approaches, particularly solid-state fermentation (SSF), to produce cellulose aerogels from agricultural waste remains an understudied area. Compared to chemical and physical methods, SSF is a more sustainable and eco-friendly approach. SSF has mild operating conditions, low energy consumption, reduced water usage and wastewater production [10]–[12]. It also has simple equipment requirements and avoids toxic chemicals [10]–[12]. Additionally, SSF can selectively remove non-cellulose components, such as hemicellulose and lignin [13]. Furthermore, SSF can result in cellulose fibers with distinct physicochemical characteristics due to specific modifications of the cellulose structure [13].

This study utilized SSF as a pretreatment before hot water treatment to increase the cellulose content of peanut shell fiber (PSF). PSF was then used in aerogel production. The process is sustainable since peanut shells were used as the sole material without added chemicals. The SSF conditions that produced the highest levels of cellulose and the lowest levels of non-cellulose components (including lignin and hemicellulose) in PSF were determined. We also evaluated the chemical composition and structural-morphological characteristics of fermented PSF (F-PSF) compared to unfermented PSF (U-PSF). Aerogels produced using PSF prepared under optimal conditions were examined for various functional properties, including density, porosity, hydrophobicity, thermal conductivity, mechanical stability, oil absorption capacity, and reusability.

2 Materials and Methods

2.1 *Materials*

2.1.1 Peanut shell

Fresh peanuts were obtained from a Vietnamese farm, which were verified as *Arachis hypogaea L.* species by the botanists at the University of Medicine and Pharmacy (Ho Chi Minh City, Vietnam).

2.1.2 Fungus

The *Aspergillus niger* strain was obtained from the microbial library at Nguyen Tat Thanh University (Ho Chi Minh city, Vietnam) and verified as *A. niger* by 18s rRNA gene sequencing.

2.1.3 Chemicals

All chemical reagents used for experiments were purchased from Sigma Aldrich (USA).

2.2 *Methods*

2.2.1 Dry material preparation

Mature peanuts (*Arachis hypogaea L.*) were harvested in August from Duc Trong District, Da Lat Province, Vietnam, and transported directly to the laboratory. Upon arrival, the peanut shells were manually separated, with only morphologically intact specimens selected for processing. These selected shells were then thoroughly washed by deionized water and subsequently dehydrated in a forced-air drying oven at 70 °C for 48 h (constant weight was achieved). Following drying, the shells were comminuted using a mechanical grinder and sieved to obtain a particle size fraction of smaller than 125 μm.

2.2.2 Fungal inoculum preparation

A. niger was grown on PDA agar plates at 31 °C for 3–4 days. Then, the fungi were collected and resuspended in a 0.9% saline solution (pH 7) to achieve a diluted suspension for SSF.

2.2.3 Solid-state fermentation

SSF experiments were conducted in 50 mL Erlenmeyer flasks covered with cotton plugs, following the procedure as previously described [14]–[17]. Each flask contained 1.5 g of dry material (DM). The flasks were sterilized and inoculated with a diluted *A. niger* suspension (10^7 spores per 1 g of DM in saline solution at pH 7) to achieve specific initial moisture contents ranging from 40% to 90%. The flasks were then incubated at specific temperatures (19, 25, 31, 37, or 43 °C) for durations ranging from 0 to 7 days. The moisture content was not monitored

throughout the fermentation process. Unfermented controls were prepared in parallel using the same procedure, except that saline solution was used instead of fungal inoculum.

The optimal SSF conditions for the highest cellulose content were determined using a one-factor-at-a-time approach. First, the optimal fermentation duration was determined. Then, the optimal initial moisture content was identified under the optimal fermentation duration. Finally, the optimal fermentation temperature was assessed under the optimal fermentation duration and initial moisture content.

2.2.4 Post-fermentation process

After fermentation, the residues (fermented or unfermented) were suspended in deionized water at a solid-to-liquid ratio of 1:10 (w/v). The suspensions were incubated in a water bath at 90 °C for 2 h, then allowed to cool to 25 °C. The mixture was then centrifuged to collect the insoluble residues. The insoluble residues were washed with distilled water and collected by centrifugation. The resulting pellet was dried in an oven at 70 °C for 48 h, after which the resulting fibers were subjected to further analysis or aerogel production. Non-hot water-treated F-PSF (NF-PSF) and U-PSF (NU-PSF) were prepared similarly, excluding the 90 °C incubation step.

2.2.5 Mild alkaline treatment of peanut shell fiber

Alkaline-treated peanut shell fiber (A-PSF) was prepared using the previously described procedure [18] with modifications. Briefly, DM was mixed with a 1% (w/w) NaOH solution at a solid-to-liquid ratio of 1:10 (w/v). The mixture was incubated in a water bath at 90 °C for 2 h and then processed in the same manner as in 2.2.4.

2.2.6 Fiber yield and lignocellulosic content

The fiber yield was quantified using Equation (1).

$$\text{Yield (\%)} = \frac{W_{PSF}}{W_{PS}} \text{ x } 100 \quad (1)$$

where W_{PSF} is the weight of dry PSF, and W_{PS} is the weight of dry peanut shell powder. The hemicellulose, lignin, and cellulose content of the fiber samples were determined as previously described [19].

2.2.7 Scanning electron microscopy (SEM)

We examined the microstructural morphology using a field emission scanning electron microscope (FE-SEM S-4800), following the previously described procedure [20]. To enhance surface conductivity prior to imaging, the samples were sputter-coated with a thin layer of platinum for 30 s.

2.2.8 X-ray diffraction and crystallinity

X-ray diffraction (XRD) analysis was performed following a previously established methodology [21]. Measurements were conducted using an X-ray diffractometer operating at 40 kV and 30 mA with Cu Kα radiation (wavelength λ = 1.540598 Å). Data were acquired over a 2θ range of 5° to 90°, with a step size of 0.02°. The crystallinity index (%CI) was calculated using Equation (2).

$$\%CI = \frac{I_{002} - I_{am}}{I_{002}} \text{ x } 100 \quad (2)$$

where I_{002} represents the diffraction peak intensity corresponding to the (002) crystallographic plane ($2\theta \approx 22°$), and I_{am} denotes the diffraction intensity associated with the amorphous region ($2\theta \approx 18°$). Crystallite size (D) was determined from XRD data following the Debye-Scherrer equation (Equation 3).

$$D = \frac{k \text{ x } \lambda}{\beta \text{ x } \cos\theta} \quad (3)$$

where k is the Scherrer constant (approximated as 0.9), λ is the wavelength of the X-ray radiation used, β denotes peak broadening at full width at half maximum, and θ is the Bragg angle.

2.2.9 Fourier transform infrared spectroscopy

Fourier Transform Infrared Spectroscopy (FTIR) analysis was performed following a previously established methodology [20]. FTIR measurements were carried out on an Agilent Cary 630 FTIR Spectrometer equipped with an Attenuated Total Reflectance (ATR) accessory, utilizing a platinum crystal plate.

2.2.10 Aerogel production

The aerogel assembly was carried out using a modified version of the previously established methodology [1]. Briefly, 0.15 g of fibers was

dispersed in 50 mL of the binder mixture while stirring continuously at 80°C. The binder mixture contained two agents: polyvinyl alcohol (PVA) and xanthan gum (XTG). The final concentrations of these agents were 0.3% and 0.15%, respectively. To ensure homogeneity and prevent air bubbles, the mixture underwent ultrasonic treatment for 15 min. The resulting suspension was aged in an oven at 70 °C for 2 h, a process indicated to promote cross-linking between the PVA/XTG matrix and the cellulose fibers, thereby increasing structural stability [1]. The cellulose suspension was maintained at -20 °C for 24 h, after which the frozen samples were sublimated under vacuum using a freeze dryer (5 Pa, 48 h). The resulting aerogel was stored in a desiccator for subsequent experiments.

2.2.11 Aerogel bulk density

The bulk density (ρ) of the aerogels was determined by measuring the mass and volume of cylindrical specimens, as previously described [1], and calculated using Equation (4).

$$\rho = \frac{m}{V} \quad (4)$$

where m represents the measured mass of the aerogel specimen and V is its corresponding volume.

2.2.12 Aerogel porosity

The porosity φ (%) of aerogels was determined as previously described [1] by Equation (5).

$$\varphi = (1 - \frac{\rho_a}{\rho_b}) \times 100 \quad (5)$$

where ρ_a (g/cm³) is the bulk density of the aerogel, and ρ_b is the average density of the aerogel components, calculated by Equation (6).

$$\rho_b = \frac{C_{PSF} + C_{PVA} + C_{XTG}}{\frac{C_{PSF}}{\rho_{PSF}} + \frac{C_{PVA}}{\rho_{PVA}} + \frac{C_{XTG}}{\rho_{XTG}}} \quad (6)$$

ρ_{PSF} ρ_{PVA}, and ρ_{XTG} are the densities of the PSF, PVA (1.2 g/cm³), and XTG (1.5 g/cm³), respectively. C_{PSF}, C_{PVA}, and C_{XTG} are the mass fractions of the PSF, PVA, and XTG, respectively, in the aerogel.

2.2.13 Aerogel hydrophobicity

The hydrophobicity of aerogel samples was evaluated using the previously described method of measuring the water contact angle [22]. A droplet of water was gently deposited onto the surface of each aerogel, and an image was immediately captured to determine the contact angle.

2.2.14 Aerogel thermal conductivity

The TCi thermal conductivity analyzer (C-Therm Technologies, Canada) was employed to determine the thermal conductivity of aerogels.

2.2.15 Aerogel oil absorption

The oil absorption capacity (q) of the aerogels was evaluated as previously described with modifications [23]. The absorption capacity, q (g/g), was determined using Equation (7).

$$q = \frac{m_1 - m_0}{m_0} \quad (7)$$

where m_1 (g) and m_0 (g) represent the weight of the aerogel after and before oil absorption, respectively.

2.2.16 Aerogel compression testing

The compressive test for aerogels was performed as previously described [23]. In brief, an aerogel of a specific height (h_0, mm) was compressed by a 5 kg weight for 1 min. Then, after 3 min, the compression was released and the height of the aerogel (h_1, mm) was measured. The size restoration level was calculated using Equation (8).

$$\text{Size restoration (\%)} = \frac{h_1}{h_0} \times 100 \quad (8)$$

2.2.17 Statistical analysis

Significant differences between the two groups were determined by Student's t-test. For assessing statistical differences among three or more independent groups, one-way ANOVA followed by Tukey's HSD test was used. All tests were performed with the R program (version R 4.5.0). A difference was considered significant if the *p*-value was less than 0.05.

3 Results and Discussion

3.1 *Effects of fermentation conditions on lignocellulosic content of peanut shell fiber*

This study investigated the effects of three SSF conditions on the lignocellulosic content of PSF. The conditions examined were fermentation duration, initial moisture content, and temperature. The ranges examined for these conditions were based on previously reported conditions suitable for *A. niger* growth [10]–[12]. The first condition assessed was fermentation duration. While the overall yield of fiber extraction remained the same between F-PSF and U-PSF throughout the 7-day period (Figure 1), a notably higher cellulose content was observed in F-PSF at days 6 and 7 in comparison to U-PSF (Figure 1). In contrast, there was a concomitant reduction in the levels of hemicellulose and lignin after 6-day fermentation (Figure 1). The results suggest that fermentation pretreatment effectively removes non-cellulosic components, thereby enhancing the purity of the extracted cellulose. Prior research has demonstrated the efficacy of *A. niger* in reducing the hemicellulose and lignin content of other lignocellulosic feedstocks (e.g., rice bran) by secreting hemicellulases and ligninases over a 7-day fermentation period [11]. However, the process takes too long to be economically viable for industrial applications. The time efficiency could be improved by using advanced bioreactors with efficient heat dissipation and mass transfer systems, selecting microbial strains that effectively produce lignocellulosic enzymes, or optimizing the pretreatment process before SSF.

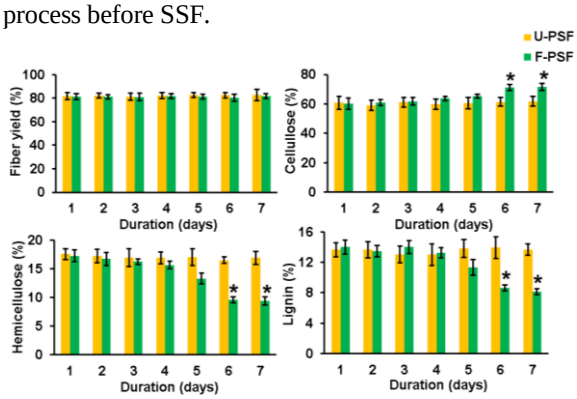


Figure 1: Effects of fermentation duration on fiber yield and lignocellulosic components. SSF conditions were fixed (70%, 31 °C) except for the varied fermentation duration. Data were mean ± standard deviation from three independent experiments; *significant difference from all unmarked groups.

The mechanism by which *A. niger* increases cellulose content likely involves its ability to disrupt rigid cell walls and remove non-cellulosic components [11]. Hemicellulose and lignin, with their less ordered structure, are generally more susceptible to enzymatic degradation than cellulose [24]. Conversely, the linear β-1,4-glucan chains of cellulose are tightly packed through extensive intra- and intermolecular hydrogen bonding. These interactions form a highly crystalline structure that is significantly resistant to enzymatic hydrolysis. Additionally, hemicellulose and lignin have more exposed surfaces than cellulose, making them more accessible to lignocellulolytic enzymes. Consequently, the enzymatic action preferentially targets and breaks down hemicellulose and lignin while leaving the cellulose proportion largely intact. Controlling fermentation duration is critical, as prolonged fermentation may decrease cellulose content.

Since the increase in cellulose content was achieved after 6 days of fermentation, the fermentation was performed for 6 days to evaluate the effect of the next parameter, initial moisture content. Optimal moisture content is crucial for maintaining the turgor pressure within the fungal hyphae, which facilitates nutrient transport and supports metabolic processes essential for enzyme synthesis and secretion [25]. Notably, the highest percentages of cellulose were observed at initial moisture levels of 80% and 90% (Figure 2). Concomitantly, at these moisture points, a significant reduction in the proportions of lignin and hemicellulose was evident. This inverse relationship suggests that an initial moisture content within the range of 80–90% possibly provides a conducive environment for fungal growth, along with the production and activity of lignocellulolytic enzymes. Since there was no monitoring of the moisture content throughout the fermentation process, inevitable evaporation loss might negatively affect the fungal growth. Maintaining the moisture content for optimal fungal growth during fermentation may require a combination of precise humidity control, water replenishment strategies, and bioreactor engineering.

The final parameter examined was fermentation temperature. The SSF was performed at the optimal duration and moisture condition as determined above. A fermentation temperature of 31 °C represents a pivotal point where cellulose, hemicellulose, and lignin content diverge significantly from the trends observed at other temperatures (Figure 2). This distinct compositional shift at 31 °C suggests that this

temperature plausibly provides optimal conditions for the synthesis and activity of hemicellulose- and lignin-hydrolytic enzymes. This observation aligns with previous research identifying 31 °C as an optimal temperature for *A. niger* SSF to break down lignocellulosic biomass [2], [12]. Overall, the optimal conditions for SSF to enhance the cellulose content and reduce the non-cellulosic content of peanut shell fiber were identified as a fermentation duration of 6 days, an initial moisture content of 80%, and a temperature of 31 °C. Under these conditions, F-PSF has significantly higher cellulose content and lower hemicellulose and lignin content than U-PSF (Table 1).

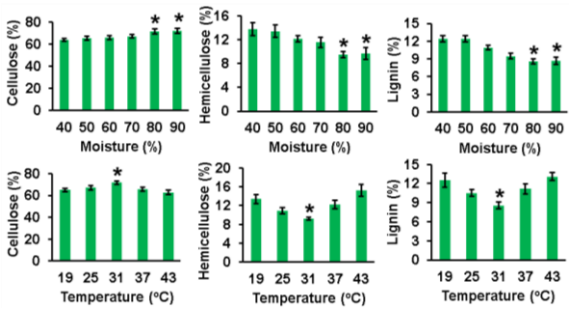


Figure 2: Effects of initial moisture content and temperature on lignocellulosic components. All SSF conditions were fixed (6 days, 80%, 31 °C) except the varied condition. Data were mean ± standard deviation from three independent experiments; *significant difference from all unmarked groups.

Table 1: Physicochemical characteristics of peanut shell fiber.

	U-PSF	F-PSF
Cellulose (%)	59.08 ± 3.61	71.76 ± 2.11*
Hemicellulose (%)	17.25 ± 1.20	9.25 ± 0.30*
Lignin (%)	13.67 ± 1.07	8.56 ± 0.54*
CI (%)	64.25 ± 1.36	78.42 ± 2.31*
Crystal thickness (nm)	2.48 ± 0.17	4.21 ± 0.20*

Data were mean ± standard deviation from three independent replicates; *significant difference from U-PSF.

Since SSF was followed by hot water treatment, the observed effect was likely due to the combined influence of both processes. In fact, the integrated SSF and hot water treatment was more effective than SSF alone at removing hemicellulose and lignin (Table 2). Hot water treatment alone, however, had a negligible effect. Notably, the SSF-hot water treatment combination was more efficient at removing hemicellulose and lignin than mild alkaline treatment (Table 2). Thus, this study underscores the efficacy of this eco-friendly hybrid process in refining cellulose fiber from lignocellulosic biomass.

Table 2: Effects of different treatments on hemicellulose and lignin content.

	Hemicellulose (%)	Lignin (%)
A-PSF	11.72 ± 0.43*	10.13 ± 0.32*
NU-PSF	18.14 ± 0.76	14.44 ± 0.70
NF-PSF	12.24 ± 0.62*	10.95 ± 0.43*
U-PSF	17.60 ± 1.06	14.26 ±0.69
F-PSF	9.21 ± 0.40	8.65 ± 0.45

Data were mean ± standard deviation from three independent replicates; *significant difference from all unmarked groups in the same column.

Beyond hot water treatment, SSF could integrate with physical and chemical treatments to enhance its efficiency. Various physical approaches can be implemented, such as mechanical comminution, steam explosion, hydrothermal pretreatment and irradiation [26]–[28]. Chemical approaches utilize specific reagents to break down ester and ether linkages within the lignocellulosic complex, leading to the solubilization or modification of lignin and hemicellulose. Prevalent chemical pretreatments include acid, alkaline, oxidative, organosolv, ionic liquid and deep eutectic solvent pretreatment [29]–[31].

Beyond *A. niger*, other fungi can be used in SSF for lignocellulose deconstruction. White-rot fungi, such as *Phanerochaete chrysosporium* and *Trametes versicolor*, are particularly adept at degrading lignin due to their extracellular ligninolytic enzymes, including lignin peroxidase, manganese peroxidase, and laccases [32]. These fungi can selectively remove lignin while leaving cellulose and hemicellulose relatively intact. However, these processes are typically slow, often requiring weeks to months for significant effects. In contrast, brown-rot fungi primarily degrade cellulose and hemicellulose with limited lignin degradation [32]. While generally less efficient than fungal systems, certain bacteria, including *Rhodococcus*, *Pseudomonas*, and *Streptomyces* species, have the ability to degrade lignin. They offer advantages in terms of broader operational conditions and ease of management compared to fungal systems [33].

Compared to microbial fermentation, enzymatic pretreatment is highly selective, efficient, and eco-friendly. It involves the action of purified ligninolytic or hemicellulolytic enzymes under mild conditions. However, the high cost of producing enzymes and the challenges related to their stability, especially on an industrial scale, remain significant limiting factors.

3.2 *Physicochemical characteristics of peanut shell fiber*

3.2.1 X-ray diffraction analysis

With respect to the XRD diffractogram of U-PSF, a broad amorphous halo was observed (Figure 3(a)), which was likely attributed to the significant presence of lignin and hemicellulose. These inherently amorphous polymers constitute a significant portion of the untreated biomass and lack a regular, repeating structure necessary for sharp diffraction peaks [34]. Whereas the XRD spectrum of F-PSF exhibits more defined, albeit still broad, diffraction features centred around 15°, 22°, and 35° in 2θ (Figure 3(a)). These angular positions are characteristic reflections of cellulose [35]. The relatively clearer cellulose features in F-PSF can be explained by the lower content of lignin and hemicellulose. A reduction of the overall amorphous background scattering allows the cellulose diffraction to become more prominent. This observation aligns with the premise that the removal of amorphous components allows for a more pronounced detection of the existing cellulose crystalline domains [18], [36]. Furthermore, the crystallinity index (CI) is higher for F-PSF (78.42%) than for U-PSF (64.25%) (Table 1), suggesting that the cellulose in F-PSF has a higher degree of crystallinity compared to the cellulose in U-PSF. The crystal thickness is also significantly larger for F-PSF (4.21 nm) compared to U-PSF (2.48 nm) (Table 1). Thus, the fermentation process plausibly facilitates better growth and ordering of the cellulose crystallites. The findings in this study are consistent with those in previous studies, indicating a higher proportion of ordered cellulose in the fermented fiber than in the unfermented fiber [37], [38].

3.2.2 Fourier transform infrared spectroscopy analysis

FTIR analysis revealed significant structural differences between F-PSF and U-PSF (Figure 3(b)). At 3300–3200 cm^{-1}, a broad and intense band was prominent in both spectra, assigned to the O-H stretching vibrations of hydroxyl groups in cellulose and hemicellulose [39]. However, the band in the F-PSF spectrum appeared slightly less intense or narrower in its trough compared to the U-PSF spectrum. This subtle alteration could imply changes in hydrogen bonding due to fermentation, potentially indicating a more open structure. A critically important observation was made at 1735 cm^{-1}, where a shoulder or weak peak was present in the U-PSF spectrum, typically attributed to the C=O stretching of acetyl and uronic ester groups in hemicellulose, or unconjugated carbonyl groups in lignin [40]. Crucially, this peak appeared significantly reduced or almost absent in the F-PSF spectrum. This observation indicates that the fermentation process likely degrades or removes a substantial portion of hemicellulose, particularly its acetyl components. The 897 cm^{-1} band, assigned to the C-H deformation of β-glycosidic linkages in cellulose, is referred to as the "amorphous cellulose" or "cellulose II" band [40]. The relative intensity and shape of this peak also appear quite similar between F-PSF and U-PSF. This observation suggests that the amorphous regions of cellulose and the presence of cellulose II polymorph, are largely maintained after fermentation. Overall, the FTIR analysis is consistent with the chemical composition and XRD analysis. It demonstrates that under optimal conditions, the fermentation process primarily induces the degradation of non-cellulosic components while maintaining the structural integrity of the fundamental cellulosic backbone.

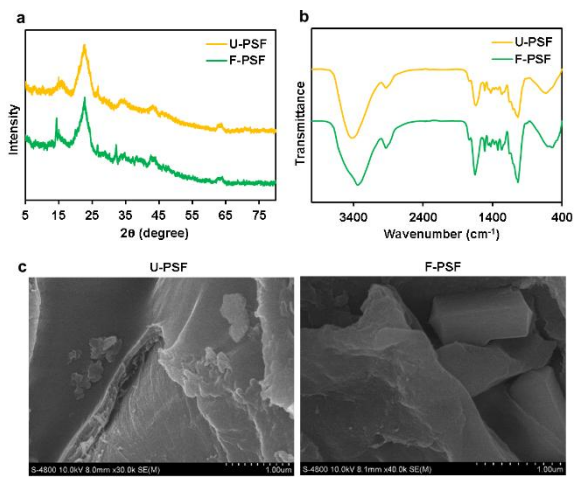


Figure 3: Physicochemical characterization of peanut shell fiber. (a) XRD spectrum; (b) FTIR spectrum; (c) SEM images.

3.2.3 Scanning electron microscopy analysis

SEM revealed that the surface of U-PSF is rough and heterogeneous, characterized by layered, sheet-like components and irregularly adhering particles (Figure 3(c)). This complex morphology likely reflects the intricate association of cellulose, hemicellulose, and lignin within the native biomass. In this unprocessed state, the intertwined biopolymers potentially obscure

the underlying cellulose structure. In contrast, F-PSF showed a more clearly defined surface with clear, separate structures. These structures likely represent the exposed fibrous structure of cellulose. This is the result of the removal of amorphous components, particularly lignin and hemicellulose, during fermentation [40]. The transformation of the fiber surface morphology after fermentation aligns with the XRD and compositional analysis results described above. These alterations may contribute to the distinct properties of the aerogels prepared from the corresponding fibers.

3.3 *Physical and oil absorption properties of aerogels from peanut shell fiber*

F-PSF and U-PSF were used to produce F-PSF aerogel (F-PSFA) and U-PSF aerogel (U-PSFA), respectively. As shown in Table 3 and Figure 4(a), F-PSFA has a significantly lower density and higher porosity than U-PSFA, indicating a lighter and more interconnected pore network. This is likely due to the increased cellulose content and decreased hemicellulose and lignin content in F-PSF. This finding aligns with previous studies reporting lower density and higher porosity in aerogels made from fibers with reduced hemicellulose and lignin content [41], [42]. The elevated porosity is also consistent with the more porous and less compact microstructure of F-PSFA, as demonstrated by SEM imaging (Figure 4(b)). Furthermore, F-PSFA exhibited a higher contact angle, indicating greater hydrophobicity (Table 3, Figure 4(c)). Additionally, F-PSFA exhibited lower thermal conductivity than U-PSFA, suggesting greater potential for thermal insulation (Table 3).

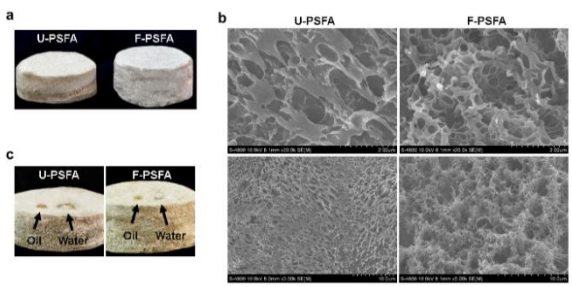


Figure 4: Aerogels from peanut shell fiber. **(**a) Images of peanut shell fiber aerogels; (b) SEM images of peanut shell fiber aerogels at different magnifications; (c) images of peanut shell fiber aerogels taken after 3 s of peanut oil or water dropping.

Table 3: Physical properties of aerogels from peanut shell fiber.

	U-PSF	F-PSF
Density (g/cm^3)	0.0333 ± 0.0017	0.0186 ± 0.0009*
Porosity (%)	90.3 ± 1.7	96.1 ± 1.9*
Water contact angle (degree)	79.3 ± 4.0	111.7 ± 6.8*
Thermal conductivity (Wm^{-1}K^{-1})	0.047 ± 0.002	0.039 ± 0.002*

Data were mean ± standard deviation from three independent replicates; *significant difference from U-PSF.

The enhancement in porosity and hydrophobicity of F-PSFA aligns with the significant improvement in the oil absorption potential for both peanut oil (PO) and diesel oil (DO) (Figure 5). Specifically, within the examined time frame of 0–180 s, F-PSFA reached maximum absorption (25 g/g for PO and 21 g/g for DO) after 60 s, whereas it took U-PSFA 120 s to reach maximum absorption (11 g/g for PO and 8 g/g for DO). This difference was significant. The substantial improvement in oil absorption potential is likely due to fermentation-mediated compositional and structural modifications of PSF. SSF selectively removes amorphous residues, thereby increasing molecular ordering and fibrillation while reducing agglomeration of the fiber structure. These changes likely result in aerogels with enhanced porosity and a more interconnected pore structure, as shown above. These improvements could create stronger capillary forces that increase oil absorption. SSF could also facilitate the chemical modification of cellulose through processes such as silanization or esterification with long-chain fatty acids [43]. Such modifications lead to increased hydrophobicity of F-PSFA. This attribute promotes stronger hydrophobic and van der Waals interactions between oil and surface molecules, enhancing the adhesion of oil molecules to the internal surfaces of the aerogels.

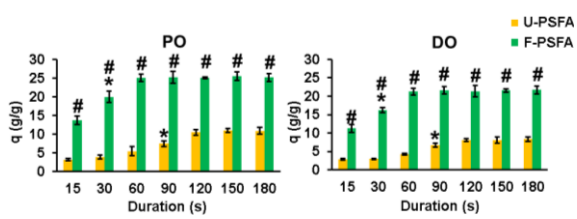


Figure 5: Oil absorption capacity of peanut shell fiber aerogels. PO: peanut oil; DO: diesel oil. Data were mean ± standard deviation from three independent replicates; *significant difference from all other groups in U-PSFA or F-PSFA; #significantly different from U-PSFA after the same duration.

In addition to high absorption capacity, long-term performance and durability are critical goals for developing oil sorbents from economic and environmental standpoints. In line with these goals, the study demonstrated the superior reusability and capacity of F-PSFA for oil absorption. While the oil absorption capacity of F-PSFA decreased from 25 g/g to 17 g/g for PO and from 21 g/g to 15 g/g for DO after the first cycle, it remained superior after nine cycles (11 g/g for both PO and DO), surpassing the capacity of U-PSFE, which was only 1 g/g for both PO and DO after nine cycles (Figure 6). The significant capacity loss observed during repeated cycles is likely caused by structural collapse. Specifically, the compression force may disrupt the intermolecular bonds that hold the three-dimensional network together, resulting in irreversible structural deformation. However, enhanced reusability of F-PSFA is attributed to improved structural stability of the porous network, enabling it to withstand mechanical stresses of compression over multiple cycles. In fact, F-PSFA exhibited higher levels of size restoration than U-PSFA up to nine compression times (Figure 7). This finding indicates the improved mechanical stability of F-PSFA and could explain its superior oil absorption capacity over multiple cycles. The structural stability of F-PSFA can be further improved by optimizing aerogel preparation parameters. Some examples of these parameters are the concentrations of PVA/XTG, the aging and drying process conditions, or the addition of binders with higher flexibility.

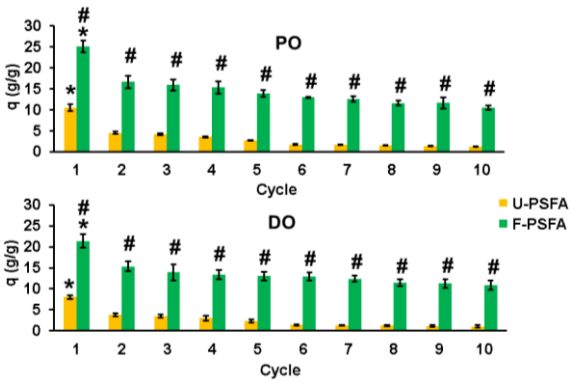


Figure 6: Reusability of peanut shell aerogel for oil absorption. PO: peanut oil; DO: diesel oil. Data were mean ± standard deviation from three independent replicates; *Significant difference from all other groups in U-PSFA or F-PSFA; #significantly different from U-PSFA for the same cycle number.

The characteristics of the F-PSFA in this study are comparable to those of cellulose aerogels prepared from other lignocellulosic sources (Table 4). The study emphasizes that the fermentation process substantially influences the physical and functional properties of PSF aerogels, which have promising applications in various fields. Further optimizing the composition of the aerogels and production parameters, especially at larger scales, may improve their properties for specific applications, such as thermal and sound insulation, and the absorption of oil, metals, organic solvents, and dyes.

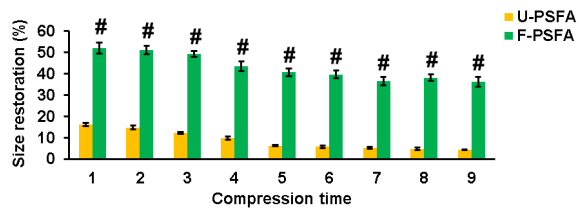


Figure 7: Size restoration ability of aerogels upon compression. #significantly different from U-PSFA after the same compression times.

Table 4: Physical properties of aerogels from different fiber sources.

Fiber source	Banana stem	Durian peel	Water hyacinth
Density (g/cm^3)	0.043	0.033	0.016
Porosity (%)	98.1	97.7	98.8
Thermal conductivity (Wm^{-1}K^{-1})	0.036	-	0.030
Oil absorption capacity (g.g^{-1})	17.4	34.9	43.2
Reference	[44]	[45]	[23]

*All performance values were mean values.

4 Conclusions

A. niger SSF was effective in removing non-cellulosic components from peanut shell fiber. The SSF conditions resulting in the highest cellulose content and lowest hemicellulose and lignin content were identified. Aerogels produced from this fiber exhibited improved physical and functional characteristics, including reduced density and thermal conductivity and enhanced porosity, hydrophobicity, mechanical stability, oil absorption capacity, and reusability. These characteristics make these materials promising alternatives in biomedicine, thermal insulation, and oil filtration. Optimizing other processing parameters to achieve specific properties of fibers and aerogels would further expand their utility as versatile, sustainable materials.

Acknowledgments

All experiments were conducted using equipment and facilities at the International University – VNU HCM.

Author Contributions

H.N.: data analysis, writing an original draft; Q.L.: data curation, data analysis, methodology. N.V.: conceptualization, data analysis, investigation, methodology, supervision, writing an original draft, writing—reviewing and editing.

Conflicts of Interest

The authors declare no conflict of interest.

Declaration of generative AI and AI-assisted technologies in the writing process

DeepL Write was used to refine the language in the manuscript.

References

[1] N. T. X. Phuong et al., "Novel fabrication of renewable aerogels from coconut coir fibers for dye removal," *Chemical Engineering Transactions*, vol. 89, pp. 31–36, 2021, doi: 10.3303/CET2189006.

[2] L.-Y. Long, Y.-X. Weng, and Y.-Z. Wang, "Cellulose aerogels: Synthesis, applications, and prospects," *Polymers*, vol. 10, p. 623, 2018, doi: 10.3390/polym10060623.

[3] X. Y. Goh et al., "Advanced fabrication and multi-properties of aluminum-based aerogels from aluminum waste for thermal insulation and oil absorption applications," *Molecules*, vol. 28, p. 2727, 2023, doi: 10.3390/molecules28062727.

[4] L. Gibowsky et al., "Conversion of natural tissues and food waste into aerogels and their application in oleogelation," *Green Chemistry*, vol. 27, pp. 4713–4731, 2025, doi: 10.1039/d4gc05703a.

[5] A.-E. Segneanu et al., "Advanced aerogels for water remediation: unraveling their potential in fats, oils, and grease sorption—A comprehensive review," *Gels*, vol. 11, pp. 268–268, 2025, doi: 10.3390/gels11040268.

[6] N. T. Vu, "Current approaches to food waste valorization for nutraceuticals," in *Sustainable Pharmaceutical Product Development and Optimization Processes*, Singapore: Springer, 2025, pp. 307–338, doi: 10.1007/978-981-97-9707-3_12.

[7] B. Koul, M. Yakoob, and M. P. Shah, "Agricultural waste management strategies for environmental sustainability," *Environmental Research*, vol. 206, 2021, Art. no. 112285, doi: 10.1016/j.envres.2021.112285.

[8] H. T. Stalker, "Peanut (*Arachis hypogaea* L.)," *Field Crops Research*, vol. 53, pp. 205–217, 1997, doi: 10.1016/S0378-4290(97)00032-4.

[9] P. Pączkowski, A. Puszka, and B. Gawdzik, "Effect of eco-friendly peanut shell powder on the chemical resistance, physical, thermal, and thermomechanical properties of unsaturated polyester resin composites," *Polymers*, vol. 13, p. 3690, 2021, doi: 10.3390/polym13213690.

[10] M. A. Guraya et al., "Impact of solid-state fermentation with *Aspergillus niger* on the chemical composition of yellow pea (*Pisum sativum* L.) flour and its application for obtaining protein products," *ACS Food Science & Technology*, vol. 5, pp. 2763–2775, 2025, doi: 10.1021/acsfoodscitech.5c00237.

[11] M. Y. Abduh, S. Alyssa, R. A. Butar, I. S. S. Pane, L. Melani, and N. I. Mohamad Puad, "Effects of solid-state fermentation using *Aspergillus niger* on yield, total phenolic content, and antioxidant activity of defatted rice bran extract," *Food Chemistry Advances*, vol. 7, Jun. 2025, Art. no. 100957, doi: 10.1016/j.focha.2025.100957.

[12] S. L. Paz-Arteaga et al., "Bioprocessing of pineapple waste for sustainable production of bioactive compounds using solid-state fermentation," *Innovative Food Science and Emerging Technologies*, vol. 85, May 2023, Art. no. 103313, doi: 10.1016/j.ifset.2023.103313.

[13] S. Magalhães et al., "Eco-friendly methods for extraction and modification of cellulose: An overview," *Polymers*, vol. 15, no. 14, p. 3138, Jul. 2023, doi: 10.3390/polym15143138.

[14] H. N. Nguyen, A. T. Huynh, M. Barcenas, T. M. Le, H. T.-K. Vu, and N. T. Vu, "Biochemical conversion of passion fruit waste into highly bioaccessible, stable, and selectively functional products," *Waste and Biomass Valorization*, vol. 16, no. 5, Jan. 2025, doi: 10.1007/s12649-024-02880-y.

[15] H. N. Nguyen, D. T. M. Chung, T. M. Le, and N. T. Vu, "Fermented *Hylocereus undatus* peel extract with enhanced antioxidant, anti-

inflammatory, anti-biofilm and sun protection Potential," *Waste and Biomass Valorization*, vol. 15, no. 12, Jul. 2024, doi: 10.1007/s12649-024-02662-6.

[16] H. T. G. Tran, H. N. Nguyen, and N. T. Vu, "Solid-state fermentation followed by maceration to recover disinfectants from aloe vera waste with improved efficacy for bacterial surface disinfection," *Waste and Biomass Valorization*, vol. 16, no. 10, pp. 5471–5485, Mar. 2025, doi: 10.1007/s12649-025-02996-9.

[17] L. V. Chau, H. N. Nguyen, T. M. Le, Q. L. Ngo, T. Nguyen, and N. T. Vu, "Fermentation-mediated enhancement of safety, thermal stability, bioaccessibility, and health-promoting potential of watermelon peel polyphenol extract," *Applied Biochemistry and Biotechnology*, vol. 197, no. 6, pp. 3748–3779, Feb. 2025, doi: 10.1007/s12010-025-05185-5.

[18] K. O. Reddy, C. U. Maheswari, M. Shukla, J. I. Song, and A. V. Rajulu, "Tensile and structural characterization of alkali treated Borassus fruit fine fibers," *Composites Part B: Engineering*, vol. 44, no. 1, pp. 433–438, Jan. 2013, doi: 10.1016/j.compositesb.2012.04.075.

[19] H. Çakmak and M. Dekker, "Optimization of cellulosic fiber extraction from parsley stalks and utilization as filler in composite biobased films," *Foods*, vol. 11, no. 23, pp. 3932–3932, Dec. 2022, doi: 10.3390/foods11233932.

[20] N. Abidi, L. Cabrales, and C. H. Haigler, "Changes in the cell wall and cellulose content of developing cotton fibers investigated by FTIR spectroscopy," *Carbohydrate Polymers*, vol. 100, pp. 9–16, Jan. 2014, doi: 10.1016/j.carbpol.2013.01.074.

[21] X. Xu et al., "Optimization of mixed fermentation conditions of dietary fiber from soybean residue and the effect on structure, properties and potential biological activity of dietary fiber from soybean residue," *Molecules*, vol. 28, no. 3, p. 1322, Jan. 2023, doi: 10.3390/molecules28031322.

[22] Z. Liang, Y. Wang, J. Xu, K. Chen, and Y. Liu, "Study on the efficient selective oil absorption and recovery of hydrophobic chitosan aerogels," *Journal of Physics: Conference Series*, vol. 2713, no. 1, Feb. 2024, Art. no. 012015, doi: 10.1088/1742-6596/2713/1/012015.

[23] T. T. V. Nguyen et al., "Synthesis, characteristics, oil adsorption, and thermal insulation performance of cellulosic aerogel derived from *Water Hyacinth*," *ACS Omega*, vol. 6, no. 40, pp. 26130–26139, Sep. 2021, doi: 10.1021/acsomega.1c03137.

[24] Z. Gaizauskaite, R. Zvirdauskiene, M. Svazas, L. Basinskiene, and D. Zadeike, "Optimised degradation of lignocelluloses by edible filamentous fungi for the efficient biorefinery of sugar beet pulp," *Polymers*, vol. 16, no. 9, p. 1178, Apr. 2024, doi: 10.3390/polym16091178.

[25] P. Ghanney, S. Yeboah, D. K. Anning, H. Yang, Y. Wang, and H. Qiu, "Moisture-induced effects on lignocellulosic and humification fractions in aerobically composted straw and manure," *Fermentation*, vol. 9, no. 6, p. 551, Jun. 2023, doi: 10.3390/fermentation9060551.

[26] D. B. Sant'Ana Júnior, M. Kelbert, P. H. Hermes de Araújo, and C. J. de Andrade, "Physical pretreatments of lignocellulosic biomass for fermentable sugar production," *Sustainable Chemistry*, vol. 6, no. 2, p. 13, Apr. 2025, doi: 10.3390/suschem6020013.

[27] E. K. Gladysheva, "Liquid hot water and steam explosion pretreatment methods for cellulosic raw materials: A review," *Polymers*, vol. 17, no. 13, pp. 1783–1783, Jun. 2025, doi: 10.3390/polym17131783.

[28] Y. Zuo, F. Zhu, S. Jiang, M. Li, and X. Kong, "Effect of electron beam irradiation pretreatment on the structure, physicochemical properties, and digestibility of starch-tannic acid complexes," *Carbohydrate Polymers*, vol. 367, Jul. 2025, Art. no. 124037, doi: 10.1016/j.carbpol.2025.124037.

[29] W.-C. Tu and J. P. Hallett, "Recent advances in the pretreatment of lignocellulosic biomass," *Current Opinion in Green and Sustainable Chemistry*, vol. 20, pp. 11–17, Dec. 2019, doi: 10.1016/j.cogsc.2019.07.004.

[30] J. Bernardo, F. Gírio, and R. Łukasik, "The effect of the chemical character of ionic liquids on biomass pre-treatment and posterior enzymatic hydrolysis," *Molecules*, vol. 24, no. 4, p. 808, Feb. 2019, doi: 10.3390/molecules24040808.

[31] V. Jančíková and M. Jablonský, "Exploiting deep eutectic solvent-like mixtures for fractionation biomass, and the mechanism removal of lignin: A review," *Sustainability*, vol. 16, no. 2, p. 504, Jan. 2024, doi: 10.3390/su16020504.

[32] J. Qi et al., "Fungal selectivity and biodegradation effects by white and brown rot fungi for wood biomass pretreatment,"

Polymers, vol. 15, no. 8, pp. 1957–1957, Apr. 2023, doi: 10.3390/polym15081957.

[33] A. Civzele, A. A. Stipniece-Jekimova, and L. Mezule, "Fungal ligninolytic enzymes and their application in biomass lignin pretreatment," *Journal of Fungi*, vol. 9, no. 7, p. 780, Jul. 2023, doi: 10.3390/jof9070780.

[34] E. Abraham et al., "Extraction of nanocellulose fibrils from lignocellulosic fibres: A novel approach," *Carbohydrate Polymers*, vol. 86, no. 4, pp. 1468–1475, Oct. 2011, doi: 10.1016/j.carbpol.2011.06.034.

[35] J. C. C.S., N. George, and S. K. Narayanankutty, "Isolation and characterization of cellulose nanofibrils from arecanut husk fibre," *Carbohydrate Polymers*, vol. 142, pp. 158–166, May 2016, doi: 10.1016/j.carbpol.2016.01.015.

[36] M. Jonoobi, J. Harun, A. Shakeri, M. Misra, and K. Oksman, "Chemical composition, crystallinity, and thermal degradation of bleached and unbleached kenaf bast (*Hibiscus cannabinus*) pulp and nanofibers," *Bioresources*, vol. 4, no. 2, pp. 626–639, Apr. 2009, doi: 10.15376/biores.4.2.626-639.

[37] J. Nsor-Atindana et al., "Enhancing the prebiotic effect of cellulose biopolymer in the gut by physical structuring via particle size manipulation," *Food Research International*, vol. 131, May 2020, Art. no. 108935, doi: 10.1016/j.foodres.2019.108935.

[38] Y. Feng, Q. Jin, X. Liu, T. Lin, A. Johnson, and H. Huang, "Advances in understanding dietary fiber: Classification, structural characterization, modification, and gut microbiome interactions," *Comprehensive Reviews in Food Science and Food Safety*, vol. 24, no. 1, Jan. 2025, Art. no. e70092, doi: 10.1111/1541-4337.70092.

[39] R. C. Kuhad et al., "Biological pretreatment of lignocellulosic biomass: An environment-benign and sustainable approach for conversion of solid waste into value-added products," *Critical reviews in environmental science and technology*, vol. 54, no. 10, pp. 771–796, Nov. 2023, doi: 10.1080/10643389.2023.2277670.

[40] S. Y. Oh, D. I. Yoo, Y. Shin, and G. Seo, "FTIR analysis of cellulose treated with sodium hydroxide and carbon dioxide," *Carbohydrate Research*, vol. 340, no. 3, pp. 417–428, Feb. 2005, doi: 10.1016/j.carres.2004.11.027.

[41] R. Morcillo-Martín, E. Espinosa, L. Rabasco-Vílchez, L. M. Sanchez, J. de Haro, and A. Rodríguez, "Cellulose nanofiber-based aerogels from wheat straw: Influence of surface load and lignin content on their properties and dye removal capacity," *Biomolecules*, vol. 12, no. 2, p. 232, Feb. 2022, doi: 10.3390/biom12020232.

[42] X. Wang et al., "Enhanced mechanical stability and hydrophobicity of cellulose aerogels via quantitative doping of nano-lignin," *Polymers*, vol. 15, no. 5, p. 1316, Mar. 2023, doi: 10.3390/polym15051316.

[43] M. A. Bryszewska, D. G. Pareja, L. Kaczmarek, A. Sobczyk-Guzenda, Malgorzata Piotrowska, and D. Batory, "SCOBY Cellulose-based materials hydrophobized using stearic acid and apple powder," *International Journal of Molecular Sciences*, vol. 25, no. 24, p. 13746, Dec. 2024, doi: 10.3390/ijms252413746.

[44] Q. N. D. Chau, Q. T. M. Le, H. K. P. Huynh, and S. T. Nguyen, "Fabrication of cellulose-based aerogel from banana stem for thermal insulation and water treatment," *IOP Conference Series: Earth and Environmental Science*, vol. 1226, no. 1, Aug. 2023, Art. no. 012023, doi: 10.1088/1755-1315/1226/1/012023.

[45] T. T. Nguyen, H. L. T. Phu, L. H. Ba, and T. V. Nam, "Synthesis and properties of cellulose aerogels from durian peel for oil adsorption," *Journal of Environmental Engineering and Science*, pp. 1–9, Dec. 2025, doi: 10.1680/jenes.25.00018.